The Diffusion Region in Collisionless Magnetic Reconnection

Michael Hesse[1], Thomas Neukirch[2], Karl Schindler[3], Masha Kuznetsova[1], and Seiji Zenitani[1]
[1]Space Weather Laboratory, NASA Goddard Space Flight Center, Greenbelt, Maryland
[2]University of St Andrews, Scotland, UK
[3]Ruhr-Universitaet Bochum, Germany

Abstract

A review of present understanding of the dissipation region in magnetic reconnection is presented. The review focuses on results of the thermal inertia-based dissipation mechanism but alternative mechanisms are mentioned as well. For the former process, a combination of analytical theory and numerical modeling is presented. Furthermore, a new relation between the electric field expressions for anti-parallel and guide field reconnection is developed.

1. Introduction

Magnetic reconnection is often recognized to be the most important plasma transport and energy conversion process in space physical plasmas. Magnetic reconnection is a likely contributor to the formation and ejection of coronal mass ejecta (e.g., Gosling et al., 1995; Antiochos et al., 1999) and to coronal heating (e.g., Forbes and Priest, 1987, Cargill and Klimchuk, 1997), and facilitates the entry of solar wind plasma and electromagnetic energy into the magnetosphere by either low- or high-latitude magnetopause reconnection (e.g., Paschmann et al., 1979; Sonnerup et al., 1981). In the magnetosphere proper magnetic reconnection converts energy stored in the magnetotail lobes to plasma internal and kinetic energy. It is also believed to play a role in the formation of the auroral acceleration region (Atkinson, 1978; Haerendel, 1987). Therefore, magnetic reconnection constitutes a fundamental and ubiquitous element of the Sun-Earth connected system.

Magnetic reconnection relies on the presence of a diffusion region, where collisionless or collisional plasma processes facilitate the changes in magnetic connection through the generation of dissipative electric fields. This diffusion region is strongly localized, extending at most to typical ion Larmor radii. Typical indirect reconnection signatures (contrasted with direct observations of the diffusion region) include the presence of fast flows and plasma heating associated with magnetic field signatures indicative of the establishment of new magnetic connections. Such indirect signatures are observed remotely in the solar corona, in the solar wind by the magnetic topology of CMEs, and by direct spacecraft observations at the magnetopause and in the magnetotail of the Earth.

In collisionless plasmas, which we identify with plasmas where collisions are sufficiently infrequent to provide the necessary dissipation on the time and spatial scales under consideration, the nature of the dissipation underlying magnetic reconnection is

ter regimes, both in regions of low magnetic field, and in the presence of a magnetic guide field.

In this paper, we present an overview of our present understanding of how particles become demagnetized in the diffusion region of the reconnection process. The emphasis of the discussion will be on electrons – however, we point out that many results apply equally to ions, after a suitable change of charge and mass. The paper will focus primarily on the thermal- or bulk inertia-based dissipation processes that have been validated in a large number of numerical models. For completeness, however, we will also mention relevant other processes, such as wave-particle interactions that have been proposed as candidate dissipation mechanisms as well.

The structure of the present paper is as follows: Following an introduction of the model in the next section, in section 3, we will present a revised theory of guide-field magnetic reconnection. Section 4 presents an analysis of our present knowledge of anti-parallel magnetic reconnection. Both sections will include summaries of translationally invariant and fully three-dimensional models. Finally, section 5 will feature a summary and a presentation of open questions that pertain to diffusion region physics.

2. The model and modeled configuration

Most of the results presented in this overview are based on the application of particle-in-cell codes. The system studied by many researchers is similar to that selected in the GEM reconnection challenge (Birn et al., 2001). This system is described in the following.

During the discussions, we will employ dimensionless quantities. For this purpose, we normalize densities by a typical density n_0 in the current sheet, the magnetic field by the asymptotic value of the reconnection magnetic field B_0. Ions are assumed to be protons (mass m_p) throughout, and length scales by the ion inertial length c/ω_i, where the ion plasma frequency $\omega_i = \sqrt{e^2 n_0 / \varepsilon_0 m_p}$ is evaluated for the reference density. Velocities are measured in units of the ion Alfven velocity $v_A = B_0 / \sqrt{\mu_0 m_p n_0}$ based on the reference magnitudes of magnetic field and density. The electric field is measured in units of $E_0 = v_A B_0$, the pressure in units of $p_0 = {B_0}^2 / \mu_0$, and the current density is normalized to $j_0 = \omega_i B_0 / c\mu_0$.

The poloidal magnetic field, a modified Harris sheet (Harris, 1962) with a current sheet half width of half the ion inertial length, is of the following form:

$$B_x = \tanh(2z) + a_0 \pi/L_z \cos(2\pi x/L_x)\sin(\pi z/L_z) \qquad (4a)$$

$$B_z = -a_0 2\pi/L_z \sin(2\pi x/L_x)\cos(\pi z/L_z) \qquad (4b)$$

The perturbation amplitude a_0=0.1 leads to an initial value of the normal magnetic field of about 3% of B_0. Similar to earlier studies (Hesse et al., 2002), we here employ a constant magnetic field component directed along the main current flow

$$B_y = B_{y0} \qquad (5)$$

where B_{y0} is the initial value of the guide field magnitude. The choice of ion-electron mass ratio varied by study; it ranges from $m_i/m_e = 25.$ in the original GEM challenge problem to $m_i/m_e = 1836$ in implicit particle-in-cell calculations (Ricci et al.,

focus on one representative timestep, $t=16$, The magnetic field and y-directed current density are shown in Figure 1. The initial, X-type perturbation leads to a reconfiguration. The most prominent difference to anti-parallel merging is the inclination of the reconnecting current sheet with respect to the X-axis. The figure also indicates the presence of a very thin current sheet in the central reconnection region, which is likely associated with electron demagnetization.

The most interesting locations for the calculation of the electron distributions are those where the electron pressure anisotropy provides the reconnection electric field. Figure 2 shows the relevant nongyrotropic components of the tensor, obtained from

$$\vec{\vec{\mathbf{P}}}_{eng} = \vec{\vec{\mathbf{P}}}_{e} - \vec{\vec{\mathbf{P}}}_{eg} \tag{8}$$

with

$$\vec{\vec{\mathbf{P}}}_{eg} = p_{\perp}\vec{\vec{\mathbf{1}}} + \frac{p_{\parallel} - p_{\perp}}{B^2}\vec{B}\vec{B} \tag{9}$$

where enq. (9) represents the gyrotropic component to the full electron pressure tensor. Figure 2 shows a strong localization of the pressure nongyrotropy near the current sheet and magnetic field reversal in the green region of fig. 1.

The thinness of the current sheet is demonstrated by Figure 3, which displays a cut in the z direction across the diffusion region current sheet. The figure shows the electron current density, and the nongyrotropic contribution to the pressure tensor component P_{yze}. A comparison with the magnitude of the local collisionless skin depth, shown at the bottom, indicates that the spatial scales of both current and pressure anisotropy are smaller. We will show below that the relevant scale here is indeed given by the local electron Larmor radius.

In order to shed light on the underlying physical process, we now investigate particle distribution functions. For this purpose, we collect particle distributions at the location $13.1<x<13.2$ and $-0.01<z<0.04$ just above the reconnection region, where the nongyrotropic y-z pressure tensor component provides the gradient, which supports most of the reconnection electric field.

The relevant reduced distribution $F(v_y, v_z)$ is displayed in Figure 4. Here, the green arrow indicates the magnetic field direction, which is essentially exclusively in the y direction (B_z is negligible). In addition, the white ellipse is drawn to guide the eye in the explanation of the nongyrotropy. Specifically, we point out that there is slightly more phase space density for positive v_z than for negative v_z if v_y is large and negative, and the opposite holds for positive v_y. This slight asymmetry indicates a preference for more acceleration in the negative v_y direction if particles move away from the central current sheet, and it is sufficient to explain the nongyrotropy of P_{yze}.

Preferential acceleration for particles closer to the center of the current sheet is due to the strong localization of the parallel electric field, shown in Figure 5. The region of particle collection is marked by the black rectangle. The (electron Larmor) scale length of the electric field variation implies that particles with instantaneous gyrocenters below the observation point will have been accelerated more than those with instantaneous gyrocenters above the observation point. Accordingly, on average, particles with $v_z<0$ will have been less accelerated in the negative y direction than particles with $v_z>0$. This idea is captured in Figure 6, which shows a distribution function

pressure tensor becomes:

$$P_{yze} \approx \frac{1}{\Omega_{ey}} \frac{\partial Q_{xyze}}{\partial z} \tag{13}$$

Further progress therefore requires an analytic expression of an evolution equation for the entire heat flux tensor. The heat flux tensor is defined in the electron center-of-mass system as:

$$\ddot{\mathbf{Q}} = m_s \int d^3u (\vec{u} - \vec{v})(\vec{u} - \vec{v})(\vec{u} - \vec{v}) f_s \tag{14}$$

Here, f_s and m_s denote the distribution function and mass of plasma species s, $\vec{u}$ the phase space velocity, and $\vec{v}$ the bulk flow speed. An evolution equation for $\ddot{\mathbf{Q}}$ is obtained by multiplying the Vlasov equation by $\vec{u}\vec{u}\vec{u}$ and integrating over phase space. The result needs to be transformed into the center-of-mass frame of species s in order to derive an evolution equation for $\ddot{\mathbf{Q}}$. After a considerable amount of algebra, one finds for the components of the electron heat flux tensor (index e omitted for simplicity) (e.g., Goswami et al., 2005)

$$\begin{aligned}
&\frac{\partial}{\partial t} Q_{ijk} \\
&+\sum_l \frac{\partial}{\partial x_l}(\Gamma_{ijkl} + Q_{ijk} v_l) - \frac{1}{mn}\left(P_{ik} \sum_l \frac{\partial P_{lj}}{\partial x_l} + P_{jk} \sum_l \frac{\partial P_{li}}{\partial x_l} + P_{ij} \sum_l \frac{\partial P_{lk}}{\partial x_l} \right) \\
&+\sum_l Q_{lij} \frac{\partial}{\partial x_l} v_k + \sum_l Q_{ljk} \frac{\partial}{\partial x_l} v_i + \sum_l Q_{lik} \frac{\partial}{\partial x_l} v_j \\
&-\frac{e}{m} \sum_{r>s} \begin{bmatrix} [Q_{ijs} B_r - Q_{ijr} B_s] \varepsilon_{rsk} \\ +[Q_{iks} B_r - Q_{ikr} B_s] \varepsilon_{rsj} \\ +[Q_{jks} B_r - Q_{jkr} B_s] \varepsilon_{rsi} \end{bmatrix} = 0
\end{aligned} \tag{15}$$

Here ε_{ijk} is the usual, totally antisymmetric tensor. We note that the expression quoted in (Hesse et al., 2004) was incorrect. We here redevelop the subsequent theory below and we will show that the resulting approximate expression for the reconnection electric field (Hesse, 2006) remains unchanged.

Equation (15) relates the time evolution of Q_{ijk} to lower order moments such as pressure and velocities, as well as to the fourth order tensor Γ_{ijkl}. The last term in (15) represents the effects of particle cyclotron motion on the heat flux tensor. Clearly, (15) is invariant under change of order of indices, leading to a totally symmetric heat flux tensor.

Further progress toward a simple scaling relation requires simplifying assumptions. Neglecting time dependence and the 4-tensor, an expression for Q_{xyz} can be obtained from the x,y,x-component of (15)

The next step is to look at P_{xy}. The analogue to eqn. (13) is:

$$P_{xy} \approx -\frac{1}{\Omega_y}\left(\frac{\partial Q_{xyz}}{\partial x}+\frac{\partial Q_{zyz}}{\partial z}\right) \tag{25}$$

The corresponding electric field becomes, in leading order:

$$E_{y2}=-\frac{1}{en}\frac{\partial P_{xy}}{\partial x} \approx \frac{1}{en\Omega_y}\left(\frac{\partial^2 Q_{xyz}}{\partial x^2}+\frac{\partial^2 Q_{zyz}}{\partial x \partial z}\right) \tag{26}$$

The second term vanishes by symmetry. We therefore get:

$$E_{y2} \approx \frac{1}{en\Omega_y}\frac{\partial^2 Q_{xyz}}{\partial x^2} \tag{27}$$

Using a similar argument as above the tensor component becomes again:

$$Q_{xyz} \approx \frac{P_{xx}}{2\Omega_y}\vec{v}\cdot\nabla v_y + const. \tag{28}$$

The first derivative becomes, in good approximation:

$$\frac{\partial}{\partial x}Q_{xyz} \approx \frac{P_{xx}}{2\Omega_y}\left(\frac{\partial v_x}{\partial x}\frac{\partial v_y}{\partial x}+v_x\frac{\partial^2 v_y}{\partial x^2}\right) \tag{29}$$

The second derivative becomes:

$$\frac{\partial^2}{\partial x^2}Q_{xyz} \approx \frac{P_{xx}}{\Omega_y}\frac{\partial v_x}{\partial x}\frac{\partial^2 v_y}{\partial x^2} \tag{30}$$

where we have used the symmetries to eliminate some derivatives. The electric field contribution becomes, from (27):

$$E_{y2} \approx \frac{P_{xx}}{en\Omega^2}\frac{\partial v_x}{\partial x}\frac{\partial^2 v_y}{\partial x^2} \tag{31}$$

which leads to the final result:

$$enE_{y2} \approx \frac{1}{2}mnr_L^2\frac{\partial v_x}{\partial x}\frac{\partial^2 v_y}{\partial x^2} \tag{32}$$

Taking (28) and (35) together and assuming a weak density variation (consistent with the incompressibility assumption) yields:

$$E \approx \frac{1}{2en}r_L^2\frac{\partial v_x}{\partial x}\nabla^2\left(mnv_y\right) \tag{33}$$

which is the same result as Hesse (2006).

Eqn. (33) offers interesting insight into the physics of the underlying reconnection process. Based on distribution function analysis we argued above that accelerated particles preferentially leave the reconnection region, whereas particles, which have, on average, been accelerated less tend to enter. In the absence of acceleration of the reconnection electric field the current density would therefore decay – which validates our gedankenexperiment above.

Comparison with (12) reveals that the coefficient κ (analogous to a diffusion coefficient) is:

$$\kappa = \frac{1}{2}r_L^2\frac{\partial v_x}{\partial x} \tag{34}$$

This expression shows the following. First of all, the square of the Larmor radius indicates that the electric field scales with the square of the ratio of critical length scale and Larmor radius in the guide field. Clearly, this implies that the actual current layer

tion was first described by Horiuchi and Sato (1994). Hesse and Winske (1998) performed a particle-in-cell simulation of collisionless reconnection in the GEM geometry. Their analysis showed indeed the presence of electron pressure nongyrotropies near the X point. The magnitude of these tensor components proved to be sufficient to provide the reconnection electric field via the expression (3).

These studies were taken a step further by Hesse et al. (1999), who investigated the effect of different electron masses on the collisionless dissipation process in the reconnection region. The target of the investigation was to study whether different physics in the diffusion region might lead to different dissipation, thereby influencing and potentially changing the larger scale behavior of the system under investigation. In order to test the dependence of the reconnection process on the assumed electron mass, Hesse et al. (1999) performed a set of simulations with varying electron masses, ranging from $m_i / m_e = 9$ to $m_i / m_e = 100$.

We here discuss a more recent calculation, which employs $m_i / m_e = 100$. The system size is L_x=100 and L_z=50, and a total of 10^9 particles. Figure 8 shows the magnetic field evolution with the current density color-coded. Arrows indicate the locations, where particles are collected to form distribution function (see below). The figure shows that magnetic reconnection, initiated by the initial perturbation, causes large changes to the magnetic field and current density distribution. The figure demonstrates that the current density exhibits a saddle-point at the location of the reconnection region. The latter feature becomes most prominent at later times.

The relevant off-diagonal components of the pressure tensor are shown in Figure 9. Similar results were found also by many other investigations, e.g., Pritchett (2001a). It is apparent from the discussion above that the processes responsible for these electron pressures rely on the inertia of individual electrons, which contributes to all of the fluid terms on the RHS of eqn. (2).

Figure 10 shows reduced distribution functions, similar to those presented above for finite guide field, at the location indicated by arrows in fig. 8. The left panel shows $F(v_z, v_y)$ in the inflow region, and $F(v_x, v_y)$ is shown in the outflow region. Qualitatively, the figure shows the same features as the ones found in the guide field model above: On average, more hot and accelerated plasma is leaving the diffusion region than is entering. We will come back to this point below.

In order to estimate the magnitude of the reconnection electric field, Hesse et al. (1999) realized that the scale of the electron diffusion region is given by electron orbit excursion in a field reversal, the so-called "bounce width" (6). A corresponding scale can be derived for the bounce motion between the downstream magnetic field components B_z. The approximate bounce orbit is sketched in Fig. 11. This result can be used for an estimate of the electric field from (3):

$$E_y = -\frac{1}{n_e e}\left(\frac{\partial P_{xye}}{\partial x} + \frac{\partial P_{yze}}{\partial z}\right) \approx \frac{1}{n_e e}\left(\frac{P_{xye}}{\lambda_x} + \frac{P_{yze}}{\lambda_z}\right) \qquad (35)$$

Here the values of the pressure tensors are to be taken at the edges of the current sheet, where electrons begin to become magnetized. In these regions, the pressure tensor components can be approximated by (Kuznetsova et al., 1998):

$$\sqrt{2m_eT_e} \approx \frac{1}{2n_e} L^2 \frac{2m_e}{\mu_0\sqrt{2m_eT_e}} \left(\frac{\partial B_x}{\partial z}\right)^2 \tag{40}$$

We approximate the momentum density derivative in the following way:

$$\nabla^2\left(m_e n_e v_{ey}\right) \approx -\frac{2}{L^2} m_e n_e v_{ey,\max} \approx \frac{2}{eL^2} m_e j_y \approx \frac{2m_e}{e\mu_0 L^2}\frac{\partial B_x}{\partial z} \tag{41}$$

where we have neglected the electron flow velocity at the edge of the current layer and assumed that the dominant contribution to the current is by the z derivative of B_x. Assuming $L \sim \lambda_z$ as defined in (6) we get:

$$\nabla^2\left(m_e n_e v_{ey}\right) \approx \frac{2m_e}{e\mu_0\lambda_z^2}\frac{\partial B_x}{\partial z} \approx \frac{2m_e}{\mu_0\sqrt{2m_eT_e}} \left(\frac{\partial B_x}{\partial z}\right)^2 \tag{42}$$

Comparing (42) and the RHS of (40) leads to:

$$E = \frac{1}{e}\sqrt{2m_eT_e}\frac{\partial v_{ex}}{\partial x} \overset{!}{=} \frac{1}{2en_e} L^2 \frac{\partial v_{ex}}{\partial x} \nabla^2\left(m_e n_e v_{ey}\right) \tag{43}$$

the desired expression for $L \sim \lambda_z$. While we emphasize the approximate nature of the present derivation, this analysis shows that the electric field expressions (33) and (38) are of essentially the same nature.

Thus, the diffusion region in anti-parallel reconnection appears fairly well understood. However, there are other modes and instabilities that may change the reconnecting system substantially, without necessarily changing the bounce motion-based dissipation process. For example, the kinetic drift-kink instability (DKI) (Zhu and Winglee, 1996, Pritchett et al., 1996, Ozaki et al., 1996) has been suggested to substantially modify the structure of the reconnecting current sheet. Although analytical theory (Daughton, 1998, 1999) and numerical models (Hesse and Birn, 2000; Zeiler et al., 2002) show that DKI growth rates appear to be small for realistic ion-electron mass ratios, there remains some debate whether the DKI or the related sausage mode (Buechner and Kuska, 1997; Pritchett et al, 1996; Silin and Buechner, 2003) may play a role in furthering the onset of magnetic reconnection.

Finally, laboratory experiments have made great progress toward the objective to produce truly collisionless magnetic reconnection in laboratory devices. Recent studies have shown that, although (39) is reproduced in particle-in-cell simulations (Dorfman et al., 2008), laboratory measurements fail to reproduce a sufficiently strong electric field based on the same equation. This feature may be due to effects not present in the simulations models, or they may be an artifact of residual collisionality in the experiment.

5. Summary

The ability to describe the diffusion region is fundamental to our understanding of magnetic reconnection. Consequently, the dissipation region physics has attracted the attention of a substantial number of investigations. Early studies recognized that, on a microscopic level, electron orbits in the diffusion region should differ substantially from gyro-drift motions. Theoretical studies of Ohm's law in the diffusion region indicated that collisionless processes that provide reconnection electric fields should be

which, when sufficiently strong, contributes substantially to the overall pressure balance. For stronger guide fields, less plasma heating is therefore required to maintain pressure balance. This effect is evident when comparing figs. (4), (7), and (10). As expected, we find comparatively less (perpendicular) heating in the guide field model than in the anti-parallel case, where there is no guide field available to provide magnetic pressure in the diffusion region. The properties above also apply in asymmetric magnetic reconnection, even though the overall morphology may be more complex than in the symmetric cases discussed here (Pritchett and Mozer, 2009).

In summary, more research is required to provide closure to the diffusion region physics problem. It appears essential that this research be conducted by means of tailored space investigations such as those offered by NASA's Magnetospheric MultiScale (MMS) mission, and that this research be challenged by close interactions with laboratory experiments. While the ultimate answer remains elusive today, it is clear that this pursuit will be one of the most exciting endeavors in modern plasma physics.

Acknowledgments. This research was supported by NASA's MMS/SMART mission.

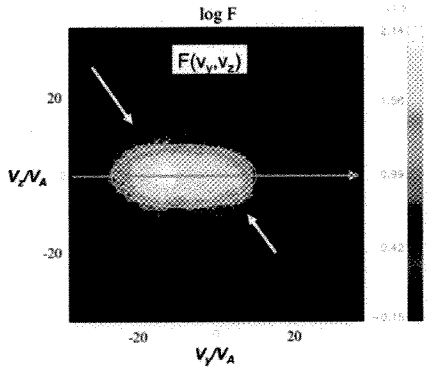

Figure 4. Reduced distribution $F(v_y, v_z)$. The distribution exhibits a small but significant nongyrotropy about the magnetic field direction green arrow, which is revealed by comparing to the white ellipse. The arrows indicate regions of enhanced electron flux.

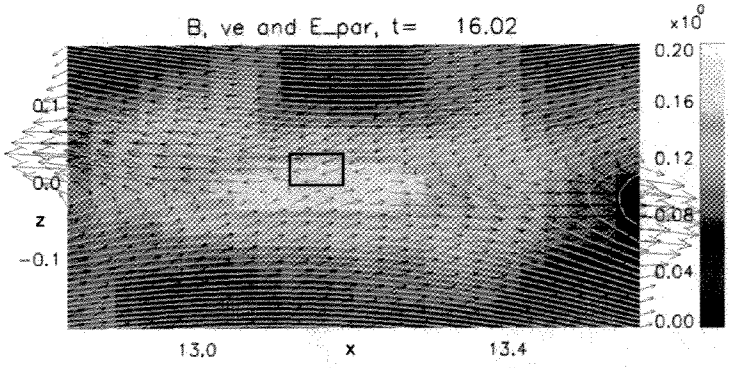

Figure 5. Parallel electric field (color), magnetic field lines (white), poloidal electron bulk flow (vectors), and particle collection box.

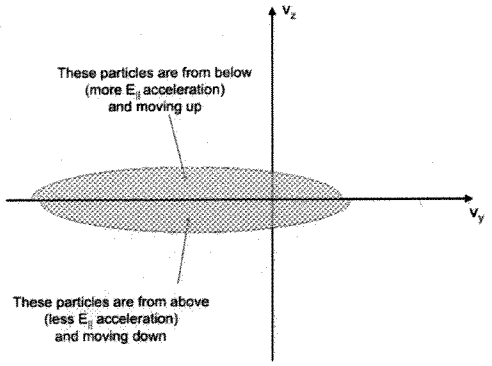

Figure 6. Illustration of the generation mechanism on the asymmetry in $F(v_y, v_z)$. Particles with gyrocenters below (in z) the dissipation region have experienced, on average, more acceleration in the negative y direction than particles with higher gyrocenters. The result is a nongyrotropy of the type shown in Fig. 4.

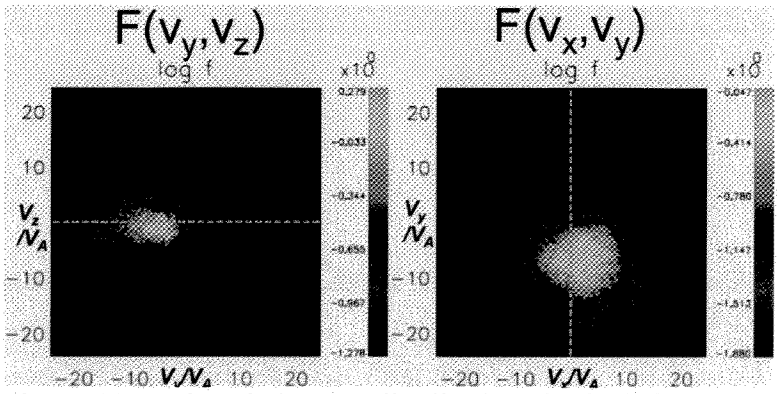

Figure 10. Reduced electron distributions in the inflow region (left) and in the outflow region (right).

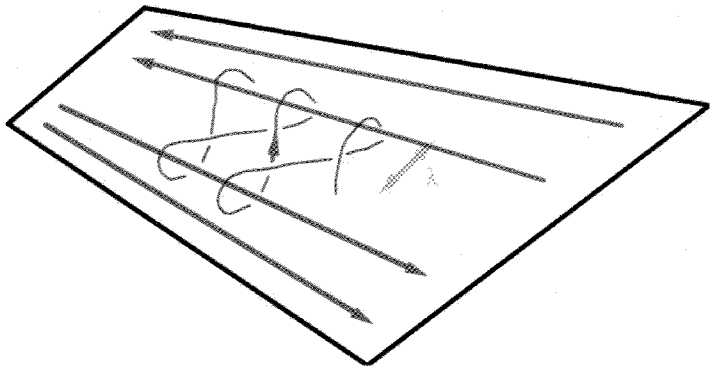

Figure 11. Schematic of the electron meandering orbits in a magnetic field reversal.

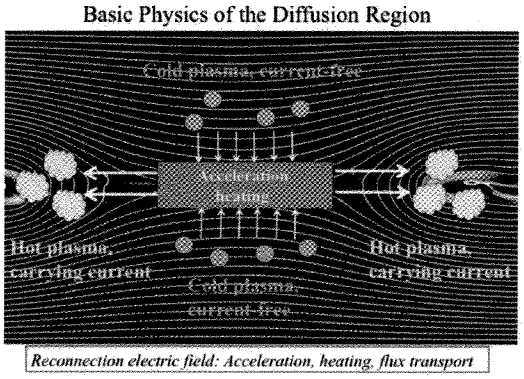

Figure 12. Schematic of the role of the reconnection electric field.

Drake, J. F., and M. E. Mandt, Structure of thin current layers: implications for magnetic reconnection, Geophys. Res. Lett., 73, 1251, 1994.

Drake, J. F., M. Swisdak, C. Cattell, M. A. Shay, B. N. Rogers, and A. Zeiler, Formation of electron holes and particle energization during magnetic reconnection, Science, 299, 873, 2003.

Forbes, T. G., and E. R. Priest, A comparison of analytical and numerical models for steadily driven magnetic reconnection, Reviews of Geophys., 25, 1583, 1987.

Gosling, J. T., J. Birn, and M. Hesse, Three-dimensional magnetic reconnection and the magnetic topology of coronal mass ejection events, Geophys. Res. Lett., 22, 869, 1995.

Goswami, P., T. Passot, and P. L. Sulem, A Landau fluid model for warm collisonless plasmas, Phys. Plasmas, 12, 102109, 2005.

Haerendel, G., On the potential role of field-aligned currents in solar physics, in Proceedings of 21st ESLAB Symposium, Bolkesjo, Norway, European Space Agency, Paris, 1987.

Harris, E. G., On a plasma sheet separating regions of oppositely directed magnetic fields, Nuovo Cim., 23, 115, 1962

Hesse, M., and D. Winske, Hybrid simulations of collisionless ion tearing, Geophys. Res. Lett., 20, 1207, 1993.

Hesse, M., and D. Winske, Hybrid simulations of collisionless reconnection in current sheets, J. Geophys. Res., 99, 11177, 1994.

Hesse, M., D. Winske, and M. M. Kuznetsova, Hybrid Modeling of collisionless reconnection in two-dimensional current sheets: Simulations, J. Geophys. Res., 100, 21815, 1995.

Hesse, M. and D. Winske, Electron dissipation in collisionless magnetic reconnection, J. Geophys. Res., 103, 26479, 1998.

Hesse, M., D. Winske, J. Birn, and M. Kuznetsova, Predictions and explanations of plasma sheet dissipation processes: Current sheet kinking, in Substorms 4, edited by S. Kokubun, and Y. Kamide, p. 437, Kluwer Academic, Boston, 1998.

Hesse, M., K. Schindler, J. Birn, and M. Kuznetsova, The diffusion region in collisionless magnetic reconnection, Phys. Plasmas, 6, 1781, 1999.

Hesse, M., and J. Birn, Near- and mid-tail current flow during substorms: Small- and large-scale aspects of current disruption, in Magnetospheric Current Systems, Geophys. Monogr. 118., edited by S. Ohtani, R. Fujii, M. Hesse and R. Lysak, p. 295, AGU, Washington, D.C., 2000.

Klimas, A., M. Hesse, and S. Zenitani, Particle-in-cell simulation of collisionless reconnection with open outflow boundaries, Phys. Plasmas, 15, 082102, 2008.

Krauss-Varban, D., and N. Omidi, Large-scale hybrid simulations of the magnetotail during reconnection, Geophys. Res. Lett., 22, 3271, 1995.

Kuznetsova, M., M. Hesse, and D. Winske, Kinetic quasi-viscous and bulk flow inertia effects in collisionless magnetotail reconnection, J. Geophys. Res., 103, 199, 1998.

Kuznetsova, M., M. Hesse, and D. Winske, Collisionless reconnection supported by nongyrotropic pressure effects in hybrid and particle simulations, J. Geophys. Res., 106, 3799, 2001.

Lin, Y., and D. W. Swift, A two-dimensional hybrid simulation of the magnetotail reconnection layer, J. Geophys. Res., 101, 19859, 1996.

Lottermoser, R.-F., M. Scholer, and A. P. Matthews, Ion kinetic effects in magnetic reconnection: Hybrid simulations, J. Geophys. Res., 103, 4547, 1998.

Lyons, L. R., and D. C. Pridmore-Brown, Force balance near an x line in a collisionless plasma, J. Geophys. Res., 95, 20903, 1990.

Ozaki, M., T. Sato, R. Horiuchi, and the Complexity Simulation Group, Electromagnetic instability and anomalous resistivity in a magnetic neutral sheet, Phys. Plasmas, 3, 2265, 1996.

Paschmann, G., et al., Plasma acceleration at the earth's magnetopause: Evidence for reconnection, Nature, 282, 243, 1979.

Pritchett, P. L., Effect of electron dynamics on collisionless reconnection in two-dimensional magnetotail equilibria, J. Geophys. Res., 99, 5935, 1994.

Pritchett, P. L., F. V. Coroniti, and V. K. Decyk, Three-dimensional stability of thin quasi-neutral current sheets, J. Geophys. Res., 101, 27413, 1996.

Pritchett, P. L., Geospace Environment Modeling (GEM) magnetic reconnection challenge: Simulations with a full particle electromagnetic code, J. Geophys. Res.,106, 3783, 2001a.

Pritchett, P. L., Collisionless magnetic reconnection in a three-dimensional open system, J. Geophys. Res., 106, 25961, 2001b.

Pritchett, P.L., and F. V. Coroniti, Three-dimensional magnetic reconnection in the presence of a guide field, J. Geophys. Res., 109, 2003.

Pritchett, P. L., and F. S. Mozer, The magnetic field reconnection site and dissipation region, Phys. Plasmas, 16, 080702, 2009.

physics, Earth Planets Spac., 53, 509, 2001.

Zeiler, A., D. Biskamp, J. F. Drake, B. N. Rogers, M. A. Shay, and M. Scholer, Three-dimensional particle simulations of collisionless magnetic reconnection, J. Geophys. Res., 107, 1230, 2002.

Zhu, Z., and R. M. Winglee, Tearing instability, flux ropes, and the kinetic current sheet kink instability in the Earth's magnetotail: A three-dimensional perspective from particle simulations, J. Geophys. Res., 101, 4885, 1996.